CONF-960848--6
ANL/XFD/CP--90675

Vibratory response of a mirror support/positioning system for the Advanced Photon Source Project at Argonne National Laboratory

Ipek Basdogan,* Thomas J. Royston,⊗ Ahmed A. Shabana,⊗
Deming Shu,* Tuncer M. Kuzay*

* Advanced Photon Source, Argonne National Laboratory, Argonne, IL 60439

⊗ Department of Mechanical Engineering, The University of Illinois at Chicago, Chicago, IL 60607

ABSTRACT

The vibratory response of a typical mirror support/positioning system used at the experimental stations of the Advanced Photon Source (APS) project at Argonne National Laboratory is investigated. Positioning precision and stability are especially critical when the supported mirror directs a high-intensity beam aimed at a distant target. Stability may be compromised by low level, low frequency seismic and facility-originated vibrations traveling through the ground and/or vibrations caused by flow-structure interactions in the mirror cooling system. The example case system has five positioning degrees of freedom through the use of precision actuators and rotary and linear bearings. These linkage devices result in complex, multi-dimensional vibratory behavior that is a function of the range of positioning configurations. A rigorous multibody dynamical approach is used for the development of the system equations. Initial results of the study, including estimates of natural frequencies and mode shapes, as well as limited parametric design studies, are presented. While the results reported here are for a particular system, the developed vibratory analysis approach is applicable to the wide range of high-precision optical positioning systems encountered at the APS and at other comparable facilities.

Keywords: vibration isolation, optics, synchrotron, positioning stability, mirror mounts, multibody systems

1. INTRODUCTION

High precision positioning is required in numerous applications, including industrial micro fabrication processes, optics, metrology, and physics research. Specific examples include the fabrication of semi-conductor-based circuits with features on the submicron level,[1] scanning electron microscopes,[2] telescopes,[3] and linear colliders.[4] In all of these cases, vibratory motion can limit the level of positioning precision that is possible. At the Advanced Photon Source (APS), a state-of-the-art synchrotron radiation facility at Argonne National Laboratory (ANL), high brilliance x-ray beams must be precisely directed through experimental stations via mirrors to distant targets. Target distances up to 30 meters with focused beam spot sizes as small as 1 mm in width are needed to support research in a wide range of technical fields, including structure of materials, X-ray imaging, and biomedical research. These mirrors are supported on positioning systems that must meet the following design requirements: (i) multi-degree of freedom (2 translational and 3 rotational) positioning capability (with accuracy on the order of microns and fractions of microradians), (ii) large load capacity, and (iii) optimal positioning stability.

Vibratory motion places a limit on positioning stability. There are three types of vibration excitation sources present at the APS facility. The first type is microseismic motion of the earth's surface. Measurements made at Argonne and other facilities with similar high precision positioning needs have shown that such extremely low level ground motion can have a detrimental effect on the facility's capabilities.[4,5] Micro-seismic motion typically ranges in frequency from 0.001 Hz to 10 Hz with an amplitude from 0.1 μm to 0.001 μm, decreasing in amplitude with increasing frequency. While these levels are within acceptable limits, dynamic

DISCLAIMER

amplification of the motion due to system resonances may result in an unacceptable amplitude of motion of the mirror. The second type of excitation sources originate in the APS facility due to machine or human activity. Vibrations caused by, for example, vacuum pumps, electric motors, or foot falls, are transmitted through the facility floor to the mirror positioning system. It is expected that the frequency range of interest due to these types of excitations will be from 0.1 Hz to 100 Hz, based on documented studies at other facilities.[4] The third type of excitation source is located in the mirror positioning system itself. Turbulent flow in the mirror cooling coils may produce vibratory motion. This phenomenon is commonly referred to as mirror jitter.[6]

Detailed vibratory studies of next generation mirror positioning systems are needed in order to understand how they will respond to these various excitation sources. Current mirror positioning system designs have been based, essentially, on the empirical knowledge of the engineers at APS. Availability of an accurate dynamic model of these systems will undoubtedly facilitate design improvements in the future.

A theoretical model for a prototypical mirror support/positioning system is proposed. It is based on a rigorous, linear multibody dynamical formulation of the equations of motion. Special care has been taken to ensure that the coupled multi-dimensional, multi-degree of freedom vibratory behavior for the entire range of positioning system configurations can be represented. Also, initial theoretical and experimental studies (when available) of the kinematic joints used in the system model are presented. Experimental studies of the stiffness and damping properties of some of these subcomponents, such as the linear screw actuators and specialized support platform bearings, are of particular importance since the validity of theoretical formulations is questionable.

Once an accurate dynamical model of the mirror positioning system is available, its response to the various vibratory excitation sources discussed above can be determined. It will be used to facilitate future design improvements that will be needed since specifications on acceptable vibration levels will continue to become more stringent as precision limitations are challenged by facility users. Since many of its components (especially the kinematic joints) as well as its overall system configuration bear resemblance to a large number of other support and positioning systems throughout the APS and similar facilities, it is expected that the insights gained through the vibratory study of this particular optical positioning system will have wide application.

2. POSITIONING SYSTEM DESCRIPTION

The novel positioning system assembly is shown in Figure 1. It consists of three main shafts attached to three precision horizontal slides arranged in a 3-point kinematic mount fashion, a pseudo- "cone-flat-V" configuration.[7] This is favored over traditional cone-flat-V designs since the sliding friction interfaces have been replaced by rolling element interfaces. The mirror is mounted on a supporting platform. This platform and a parallel lower platform are attached to the shafts using self-aligning ball bearings. As seen in Figure 2a, the slide designated "C", is fully constrained, the slide "F" is free to move in both the x and y directions, and the slide "V" is only constrained in the x direction.[8] This configuration completes the requirement for the principle of kinematics for the "cone-flat-v" 3-point kinematic mount. One translational and one rotational degree of freedom are fulfilled when the slides are driven automatically or manually (see Figure 2b). The three other degrees of freedom, vertical translational motion and two rotations are added to the design through the use of vertical actuators below the horizontal slides driven along high precision linear roller bearings. A uniqueness of this design[9] is the decoupling of the mirror from the vacuum chamber. The mirror is protected from any of the vibratory disturbances coming through the vacuum chamber through the use of flexible bellows. Another advantage of this design is that it provides significant vertical motion through the use of the main shafts since the actuators are not lifting the vacuum chamber.

3. MODELING AND ANALYSIS APPROACH

For low frequency vibrations up to a few hundred Hertz, where the amplitude of motion may be significant, some of the positioning system components may be treated as rigid while others require a flexible formulation. Additionally, the inertia of some components may be neglected. For example, the upper and lower plates have significant mass relative to the vertical shafts. Also, the vertical actuators and horizontal slides represent a significant mass concentration. These same components are significantly more rigid than the vertical shafts or bearings connecting the shafts to the plates. A list of modeling assumptions is as follows:

(1) Linear system theory valid. (Only very low amplitude motion is expected.)
(2) Upper and lower platforms are treated as rigid masses.
(3) Inner housing of the actuator mass is significant and treated as a rigid body.
(4) Shaft and bearing elements are treated as compliant and massless.
(5) Outer housing of the actuators are treated as fixed to the ground.

These assumptions are supported by theoretical and, in some cases, experimental component studies discussed in Section 4. The resulting dynamical model is shown in Figure 3. This model consists of 30 degrees of freedom (5 rigid bodies). A rigorous multibody dynamics formulation for the equations of motion is developed in Section 5. This formulation is robust in that it can predict system dynamic properties for an unlimited range of positioning configurations given the orientation of the 5 rigid bodies. In Section 6, selected results of theoretical calculations of system natural frequencies and mode shapes are provided along with some initial parametric design studies.

4. STIFFNESS COEFFICIENTS

In this section, the methods used to evaluate the stiffness coefficients of the elastic members are presented. For many of the cases, a nonlinear relationship between the deformation and applied force exists. For small perturbations about an operating point, which is typically determined by the preload, a linear approximation is valid. The stiffness coefficient is the linearized ratio between applied force and displacement.

4.1 Shaft stiffness

The three shafts are treated as massless uniform beam elements. Each node represents the translational displacements of that point on the corresponding component. Each shaft has one node on the upper platform, the lower platform and the actuator. The axial and transverse stiffness of the beam element is given by the formulas,[10]

$$(k_{shaft})_{axial} = \frac{A_{shaft} E_{shaft}}{L_{shaft}}, \qquad (k_{shaft})_{transverse} = \frac{12 E_{shaft} I_{shaft}}{L^3_{shaft}}, \tag{1a-b}$$

where E_{shaft} is the modulus of elasticity, A_{shaft} is the cross section, L_{shaft} is the length of the shaft, and I_{shaft} is the moment of inertia.

4.2 Stiffness of the linear rolling bearings in the vertical actuator

In order to calculate the stiffness components of the linear rolling bearings around the inner housing of the actuator, the Hertz Theory of Elastic contact is used.[11] The effect of geometry on the system in the contact region is a function of the algebraic sum of the curvatures of the two surfaces in contact. Thus, the contact between two surfaces can be approximated by an equivalent system having a radius

$$R_o = \frac{1}{\frac{1}{R_1} + \frac{1}{R_2}}. \tag{2}$$

The second step is to determine the equivalent modulus of elasticity of the system based on the elastic moduli and Poisson ratios of the two materials in contact. This modulus of elasticity can be evaluated as

$$E_o = \frac{1}{\frac{1-\upsilon_1^2}{E_1} + \frac{1-\nu_2^2}{E_2}}. \tag{3}$$

For a smooth circular cylinder of length l_r between two rigid planes and loaded by a force F_r, the displacement of the initial contact can be given by the formula;

$$\delta_{cyl} = \frac{2F_r}{L\pi E_o}\left[Log\left(\frac{4R_o}{b}\right) - 0.5\right], \quad \text{where } b = 2\left[\frac{F_r R_o}{\pi E_o l_r}\right]^{1/2}. \tag{4}$$

The radial force F_r on the rolling bearings is calculated based on the resulting force distribution due to the configuration of the rolling bearings around the inner housing of the actuator. The resulting spring force will be applied from two concentrated points assuming constant stiffness for each roller.

4.3 Linear stiffness of the vertical actuator

The linear stiffness of the vertical actuator is analyzed in two critical sections. The first one will be the point contact of the coupling between the lifting screw and the top plate of the actuator and the other one is the lifting screw itself.

Point Contact Stiffness: As mentioned before, the equivalent radius of the system of two surfaces in contact can be approximated using Eq. 2 and the equivalent Young moduli is given by Eq. 3. The deflection of the system due to elastic deformation of the bodies at the contact interface is[12]

$$\delta_{pc} = \frac{1}{2}\left(\frac{1}{R_e}\right)^{1/3}\left(\frac{3F}{2E_e}\right)^{2/3}. \tag{5}$$

As in the previous case, the amount of force exerted on that specific actuator is needed for the calculation of the stiffness coefficient. Three actuators carry lower and upper platforms and the three main shafts (See Fig. 1). Components of the loading force on each actuator can be calculated utilizing the static equilibrium condition of the system.

Lifting Screw Stiffness: Assuming axial deformation along the screw, the stiffness coefficient is given by the equation

$$k_{screw} = \frac{A_{screw} E_{screw}}{L_{screw}}, \tag{6}$$

where A_{screw} is the cross section, E_{screw} is the modulus of elasticity, and L_{screw} is the length of the screw. The point contact stiffness and the lifting screw stiffness will be treated as springs connected in series.

4.4 Elastic deformation of the self-aligning ball bearings

The radial and axial deformation of the roller bearings are considered. The radial deformation for the stainless steel bearing is given by the formula[13],

$$(\delta_{radial})_{SS} = \frac{0.0032}{\cos\alpha}\left(\frac{Q^2{}_{\max}}{B_d}\right)^{1/3}, \quad \text{where } (Q_{\max})_{radial} = \frac{4.37\,F_r}{2\,z\cos\alpha}. \tag{7}$$

Here, B_d is the ball diameter, α is the contact angle, and z is the number of the balls. F_r corresponds to the radial load on the bearing. The axial deformation for the stainless steel bearing is calculated in a similar fashion:

$$(\delta_{axial})_{SS} = \frac{0.0032}{\sin\alpha}\left(\frac{Q^2{}_{\max}}{B_d}\right)^{1/3}, \quad \text{where } (Q_{\max})_{axial} = \frac{F_a}{z\sin\alpha}. \tag{8}$$

Here, F_a is the axial force exerted on the bearing. In the case of ceramic bearings, deformation is given by the formulas;

$$(\delta_{radial})_{ceramic} = a\times(\delta_{radial})_{SS}, \qquad (\delta_{axial})_{ceramic} = a\times(\delta_{axial})_{SS}, \quad a = 0.891. \tag{9a-b}$$

5. MULTI-DEGREE OF FREEDOM MIRROR SUPPORT SYSTEM

The rigid body mechanics is used as the basis for developing the dynamic equations that govern the vibration of the mirror support. This methodology as well as the standard procedure used for determining the mode shapes and natural frequencies of the support system is briefly discussed.

5.1 Kinematics

Figure 4a depicts a rigid body that has a body coordinate system $X_bY_bZ_b$. The global position vector of an arbitrary point on this rigid body can be described using the translation of the reference point O_b as

$$\mathbf{r}_p = \mathbf{R} + \mathbf{A}\bar{\mathbf{u}}_p, \tag{10}$$

where $\mathbf{R}$ is the global position vector of the reference point as shown in Fig. 4a, $\mathbf{A}$ is the transformation matrix that defines the orientation of the body in the global coordinate system, and $\bar{\mathbf{u}}_p$ is a constant vector that defines the location of the arbitrary point with respect to the reference point.[14] In the case of a general three-dimensional displacement, the vector $\mathbf{R}$ is a function of three time-dependent coordinates, while the transformation matrix is a function of three independent parameters that define the rotations about the three perpendicular axes of the body coordinate system. A simple rotation ϕ about the X axis, rotation θ about the Y axis , and rotation φ about the body Z axis is described by the rotation matrix

$$\mathbf{A} = \begin{bmatrix} \cos\theta\cos\varphi & -\cos\theta\sin\varphi & \sin\theta \\ \sin\phi\sin\theta\cos\varphi + \cos\phi\sin\varphi & -\sin\phi\sin\theta\sin\varphi + \cos\phi\cos\varphi & -\sin\phi\cos\theta \\ -\cos\phi\sin\theta\cos\varphi + \sin\phi\sin\varphi & \cos\phi\sin\theta\sin\varphi + \sin\phi\cos\varphi & \cos\phi\cos\theta \end{bmatrix}. \tag{11}$$

5.2 Dynamic equations of motion

A multibody system consisting of n_b unconstrained rigid bodies has $6 \times n_b$ independent generalized coordinates. The vector $\mathbf{q}$ of the generalized coordinates of the multibody system is then defined as

$$\begin{aligned}\mathbf{q} &= \left[R_x^{\,1} \quad R_y^{\,1} \quad R_z^{\,1} \quad \phi^1 \quad \theta^1 \quad \varphi^1 \quad \ldots \quad R_x^{\,i} \quad R_y^{\,i} \quad R_z^{\,i} \quad \phi^i \quad \theta^i \quad \varphi^i \quad \ldots \right. \\ &\qquad \left. \ldots \quad R_x^{\,n_b} \quad R_y^{\,n_b} \quad R_z^{\,n_b} \quad \phi^{n_b} \quad \theta^{n_b} \quad \varphi^{n_b}\right] \\ &= \left[\mathbf{R}^1 \quad \beta^1 \quad \mathbf{R}^i \quad \beta^i \quad \ldots \quad \mathbf{R}^{n_b} \quad \beta^{n_b}\right], \end{aligned} \tag{12}$$

where $\mathbf{q}^i = \begin{bmatrix} \mathbf{R}^i \\ \beta^i \end{bmatrix}$.

The dynamic equations of motion of a rigid body, having the origin of the body coordinate system rigidly attached to the center of mass, can be written in a partitioned matrix form as[13]

$$\begin{bmatrix} \mathbf{m}^i{}_{RR} & \mathbf{0} \\ \mathbf{0} & \mathbf{m}^i{}_{\beta\beta} \end{bmatrix} \begin{bmatrix} \ddot{\mathbf{R}}^i \\ \ddot{\beta}^i \end{bmatrix} = \begin{bmatrix} \left(\mathbf{Q}^i{}_e\right)_R \\ \left(\mathbf{Q}^i{}_e\right)_\beta \end{bmatrix} + \begin{bmatrix} \mathbf{0} \\ \left(\mathbf{Q}^i{}_v\right)_\beta \end{bmatrix} \qquad i = 1,2,\ldots,n_b, \tag{13}$$

where n_b is the total number of rigid bodies in the system. The submatrices of the mass matrix associated, respectively, with the translation and orientation coordinates are $\mathbf{m}^i{}_{RR}$ and $\mathbf{m}^i{}_{\beta\beta}$. $\left(\mathbf{Q}^i{}_v\right)_\beta$ is the centrifugal force vector. $\left(\mathbf{Q}^i{}_e\right)_R$ and $\left(\mathbf{Q}^i{}_e\right)_\beta$ are the vectors of generalized forces associated, respectively, with the generalized translation and orientation coordinates.

5.3 Standard eigenvalue problem

For the free undamped case the equation of motion of a vibratory system can be written in the following form;[15]

$$\mathbf{M}\ddot{\mathbf{x}} + \mathbf{K}\mathbf{x} = \mathbf{0}. \tag{14}$$

A solution of this equation can be assumed as follows:

$$\mathbf{x} = \mathbf{X}\sin(\omega_n t + \psi), \tag{15}$$

where $\mathbf{X}$ is the vector of amplitudes, ω_n is the frequency, and ψ is the phase angle. Differentiation of Eq. 15 and substituting into Eq. 14 leads to

$$[\mathbf{K} - \omega_n{}^2\mathbf{M}]\mathbf{X} = 0. \tag{16}$$

This equation has a nontrivial solution if and only if the coefficient matrix is singular, that is,

$$\left|\mathbf{K} - \omega_n{}^2\mathbf{M}\right| = 0. \tag{17}$$

The above equation leads to a polynomial of order n in ω_n^2. The roots of this polynomial denoted as $\omega_1^2, \omega_2^2, \omega_3^2, ...\omega_n^2$ are called the *characteristic values* or the *eigenvalues*. The square roots of the eigenvalues give the natural frequencies. Associated with each characteristic value ω_i, there is an n-dimensional vector called the *characteristic vector* or the *eigenvector* X_i which can be obtained by using Eq. 16 as follows:

$$[\mathbf{K} - \omega_i^2 \mathbf{M}]\mathbf{X}_i = 0. \tag{18}$$

Equation 18 has a nontrivial solution that defines the eigenvector X_i to within an arbitrary constant. The eigenvector (amplitude) X_i is referred to as the i^{th} *mode shape* of vibration.

5.4 Definition of the generalized forces

Referring to Section 5.2, we can evaluate the mass matrix of Eq. 13 from the mass properties of the components (See Table 1). The right-hand side of the equation requires knowledge of $\left(\mathbf{Q}^i_e\right)_R$, $\left(\mathbf{Q}^i_e\right)_\beta$ and $\left(\mathbf{Q}^i_v\right)_\beta$. The forces associated with the orientation coordinates $\left(\mathbf{Q}^i_e\right)_\beta$ and the centrifugal forces $\left(\mathbf{Q}^i_v\right)_\beta$ will be calculated using the multibody formulation.[14] The vector $\left(\mathbf{Q}^i_e\right)_R$, represents the effect of the spring forces created by the elastic components of the system. These spring forces can be expressed in terms of the generalized coordinates in order to define the generalized forces in the system equations. This procedure is explained for a generalized case of two bodies connected with a spring element (Fig. 4b) and then applied to the system shown in Fig. 3.

From Eq. 10, the position vector of point P^i and P^j on two rigid bodies i and j initially (before any translation and rotation takes place) and at any instant can be written as follows,

$$\mathbf{r}_{po}{}^i = \mathbf{R}_o{}^i + \bar{\mathbf{u}}_p{}^i, \qquad \mathbf{r}_P{}^i = \mathbf{R}^i + \mathbf{A}^i \bar{\mathbf{u}}_p{}^i \tag{19a-b}$$

$$\mathbf{r}_{po}{}^j = \mathbf{R}_o{}^j + \bar{\mathbf{u}}_p{}^j, \qquad \mathbf{r}_P{}^j = \mathbf{R}^j + \mathbf{A}^j \bar{\mathbf{u}}_p{}^j. \tag{19c-d}$$

The vectors $\mathbf{R}^i$ and $\mathbf{R}^j$ can also be expressed in terms of the time-dependent body coordinates;

$$\mathbf{R}^i = \mathbf{R}_o{}^i + \begin{bmatrix} x^i \\ y^i \\ z^i \end{bmatrix}, \qquad \mathbf{R}^j = \mathbf{R}_o{}^j + \begin{bmatrix} x^j \\ y^j \\ z^j \end{bmatrix}. \tag{20a-b}$$

The component of the spring force along a line connecting points P^i and P^j can be written as

$$F_s = k(l - l_o), \tag{21}$$

where k is the spring constant, l_o is the undeformed length of the spring, and l is the current length. Here, l and l_o are defined as

$$l_o = \left|\mathbf{r}^{ij}{}_{po}\right|, \qquad l = \left|\mathbf{r}^{ij}{}_{p}\right|, \tag{22a-b}$$

where $r^{ij}{}_{po}$ and $r^{ij}{}_{p}$ are, respectively, the position vectors of point P^i with respect to point P^j, defined initially and after the deformation takes place. These vectors can be expressed in terms of the coordinates of two bodies as

$$\mathbf{r}^{ij}{}_{po} = \mathbf{r}_{po}{}^{i} - \mathbf{r}_{po}{}^{j} = \mathbf{R}_{o}{}^{i} + \bar{\mathbf{u}}^{i}{}_{p} - \mathbf{R}_{o}{}^{j} - \bar{\mathbf{u}}^{j}{}_{p} \tag{23a}$$

$$\mathbf{r}^{ij}{}_{p} = \mathbf{r}_{p}{}^{i} - \mathbf{r}_{p}{}^{j} = \mathbf{R}^{i} + \mathbf{A}^{i}\bar{\mathbf{u}}^{i}{}_{p} - \mathbf{R}^{j} - \mathbf{A}^{j}\bar{\mathbf{u}}^{j}{}_{p}. \tag{23b}$$

Then the deflection of the spring can be expressed in terms of the x, y, and z components of the corresponding vectors as follows

$$l - l_o = \left|\mathbf{r}^{ij}{}_{p}\right| - \left|\mathbf{r}^{ij}{}_{po}\right| = \sqrt{\left(x_p{}^{ij}\right)^2 + \left(y_p{}^{ij}\right)^2 + \left(z_p{}^{ij}\right)^2} - \sqrt{\left(x_{po}{}^{ij}\right)^2 + \left(y_{po}{}^{ij}\right)^2 + \left(z_{po}{}^{ij}\right)^2}. \tag{24}$$

As a first approximation, the deflection of the spring will be assumed only in the z direction. Using this assumption, the spring force vector becomes

$$\mathbf{F} = \left[0 \quad 0 \quad k(z_p{}^{ij} - z_{po}{}^{ij})\right]^T, \tag{25}$$

where the difference $z_p{}^{ij} - z_{po}{}^{ij}$ is calculated using Eqs. 20 and 23.

6. RESULTS AND DISCUSSION

Based on the modeling assumptions, theoretical calculations of the mass and stiffness properties of the system components are provided in Table 2. While a prototype of the entire system is not yet constructed, some of the off-the-shelf components are available for experimental study. For example, linear stiffness values for the self-aligning ball bearings have been dynamically measured as a function of preload and compared to values calculated from manufacturer-provided deflection formulas.[16] Fig. 5 depicts these comparisons. Further experimental studies of the bearings and the other critical kinematic joints is currently in progress.

Selected system natural frequencies and the corresponding mode shapes are computed and shown in Figure 6. Study has focused on frequencies below 400 Hz as the magnitude of displacement for frequencies beyond this range will surely fall within allowable amplitude of motion levels. It can be observed in the figure that modes corresponding to the first six natural frequencies are rotational modes about the x-y axis for the upper and lower platforms. A slight translational movement of the actuators along the z direction occurs at mode 2. Since the mirror is mounted on the upper platform, translational movement of the upper platform along the x-y axis and rotational movement about all three axes at modes 7 and 8 is important. According to the user specifications, rotation about the z axis and translation along the x axis are the most critical.[17]

One of the problems associated with the assembly is balancing the vacuum force created after the evacuation of the vacuum chamber. This can be achieved by applying a preload to the lower platform. The possible dynamic effect of this preload is simulated as an added mass to the lower platform. The first 6 frequencies are plotted in Fig. 7a as a function of the lower platform mass. Clearly, increasing lower platform mass creates an undesired effect by decreasing the resonance frequencies. The required preload might also be achieved by hanging the concentrated mass from the center of gravity of the lower platform via a very compliant element thereby minimizing its impact on the system.

Another design issue is the presence of the lower platform since it does not add additional positioning capability to the structure. To investigate its impact, it is removed. Some of the modes (3,4,5,7,8,9) are

comparable to the regular case. Other modes, such as 1, 2, and 6, have disappeared. Hence, on the one hand, the lowest system natural frequency has been increased by removing the platform, suggesting that it should not be used. On the other hand, removing the lower platform decreases the natural frequencies of the remaining modes, some of which are associated with critical motion of the upper platform. Additionally, the simplified system model used here does not account for flexibility in the outer housing of the vertical actuator or in the horizontal slides. If these are considered, then it is expected that the positive benefit of the lower platform may be more significant.

Variation in the upper platform mass was also studied (see Fig. 7c). This might occur if its shape or material were changed. Small changes in the mass do not have much effect on the lower natural frequencies since these are more associated with the lower platform. For higher resonant frequencies, increasing the mass decreases their value.

7. CONCLUSION

A generalized formulation of the system dynamic equations for support/positioning structures used in high precision optical applications has been presented. The proposed methodology considers the coupled multi-dimensional, multi-degree of freedom vibratory behavior of these complicated structures. Initial results of its application to a mirror support/positioning system to be used in the experimental stations of the APS have been presented. Natural frequencies and mode shape calculations based on theoretical estimates of the system component mass and stiffness values as well as limited parametric design studies have been discussed. For this particular system, the high natural frequencies suggest that vibratory response may not be a critical problem. However, further study is needed.

Supporting experimental analyses of available components of the system are in progress. It is expected that these studies will lead to more refined and accurate models for the stiffness and damping properties of the numerous and complex kinematic joints used in this system and in many high-precision positioning systems comparable to it at the APS facility and elsewhere. Once an accurate system model has been developed, its response to typical vibratory excitations seen during normal operation can be calculated. Limited parametric studies presented here show the potential that such a model will eventually have as an aid to designers of future support/positioning systems.

8. ACKOWLEDGEMENT

This work is supported by the U.S. department of Energy, BES-Materials Sciences, under contract no. W-31-109-ENG-38.

9. REFERENCES

1. A. Brochet and J. Bernard, "Site Selection and Design of a Low-Vibration Building for Submicron Technology Applications," *SPIE Proceedings,* Vol. 1619, pp. 148-160, 1991.
2. P.A. Jennings and J.W. Willson, "Improved Vibration Isolation System for a Scanning Electron Microscope," *SPIE Proceedings,* Vol. 1619, pp. 148-160, 1991.
3. H.M. Dyck, E. Berg and D. Harris, "A Study of Microseismic and Man-made Vibrations on Mauna Kea," *SPIE Proceedings,* Vol. 628, pp. 162-169, 1986.
4. B.A. Baklakov, et al., "Study of Seismic Vibrations for the VLEPP Linear Collider," *Technical Physics*, Vol. 38, pp. 894-898, 1993.
5. J.A. Jendrzejczyk and M.W. Wambsganss, "Vibration Considerations in the Design of the Advanced Photon Source at Argonne National Laboratory," *SPIE Proceedings,* Vol. 1619, pp. 114-126, 1991.
6. M.J. Laughlin, "Mirror Jitter: An Overview of Theoretical and Experimental Work," *Optical Engineering*, Vol. 34, pp. 321-329, 1995.
7. E. B. Wilson, *An Introduction to Scientific Research* , pp. 104-109, McGraw-Hill, 1952.
8. J. Barraza, D. Shu, and T.M. Kuzay, "Support systems for optics in the experiment stations at the Advanced Photon Source", *Nucl. Instr. and Meth.* A 347, pp. 591-597, 1994.

9. US Patent No. 5, 526, 903, June 1996.
10. J.S. Przemieniecki, *Theory of Matrix Structural Analysis*, pp. 61-80, Dover, 1968.
11. W. Flugge, *Handbook of Engineering Mechanics*, pp. 42.1-7, McGraw Hill, 1962.
12. A. H. Slocum, *Precision Machine Design*, pp. 228-233, Prentice Hall, 1991.
13. Koyo Corporation of U.S.A., personal communication, March 1996.
14. A.A. Shabana, *Computational Dynamics*, pp. 350-456, Springer-Verlag, 1994.
15. A.A. Shabana, *Theory of Vibration, Vol. 2* , pp. 91-107, Springer-Verlag, 1991.
16. T. J. Royston, et al., unpublished data, 1996.
17. W. Yun, et al., "Advantages of using a mirror as the first optical component for APS undulator beamlines," Argonne National Laboratory Report ANL/APS/TB-2, 1992.

Table 1 Submatrices of mass matrix

$m^1RR=m^4RR=m^5RR=m_{actuator}=12.71\ kg$
$m^2RR=m_{lowerplatform}=20.52\ kg$
$m^3RR=m_{upperplatform}=11.66\ kg$
$\mathbf{m}^1\beta\beta=\mathbf{m}^4\beta\beta=\mathbf{m}^5\beta\beta=\begin{bmatrix} I^1xx & I^1xy \\ I^1yx & I^1yy \end{bmatrix}=\begin{bmatrix} 7.08\times10^{-2} & 0 \\ 0 & 7.08\times10^{-2} \end{bmatrix}\ kg.m^2$
$\mathbf{m}^2\beta\beta=\begin{bmatrix} I^2xx & I^2xy & I^2xz \\ I^2yx & I^2yy & I^2yz \\ I^2zx & I^2zy & I^2zz \end{bmatrix}=\begin{bmatrix} 2.379\times10^{-1} & 4.44\times10^{-2} & 0 \\ 4.44\times10^{-2} & 9.064\times10^{-2} & 0 \\ 0 & 0 & 3.236\times10^{-1} \end{bmatrix}\ kg.m^2$
$\mathbf{m}^3\beta\beta=\begin{bmatrix} I^3xx & I^3xy & I^3xz \\ I^3yx & I^3yy & I^3yz \\ I^3zx & I^3zy & I^3zz \end{bmatrix}=\begin{bmatrix} 1.304\times10^{-1} & -2.89\times10^{-2} & 2.641\times10^{-4} \\ -2.89\times10^{-2} & 3.05\times10^{-2} & 5.422\times10^{-4} \\ 2.641\times10^{-4} & 5.422\times10^{-4} & 1.569\times10^{-1} \end{bmatrix}\ kg.m^2$

Table 2 Stiffness coefficients of the flexible components

	Cone Joint	Flat Joint	V-Joint
Shaft stiffness (N/m)	$k_{axial1}=9.648\ 10^9$ $k_{axial2}=8.744\ 10^8$ $k_{transverse1}=2.689\ 10^{10}$ $k_{transverse2}=2.001\ 10^7$	$k_{axial1}=9.648\ 10^9$ $k_{axial2}=8.744\ 10^8$ $k_{transverse1}=2.689\ 10^{10}$ $k_{transverse2}=2.001\ 10^7$	$k_{axial1}=9.648\ 10^9$ $k_{axial2}=8.744\ 10^8$ $k_{transverse1}=2.689\ 10^{10}$ $k_{transverse2}=2.001\ 10^7$
Vertical actuator linear stiffness (N/m)	$k_{act}=7.323\ 10^7$	$k_{act}=7.323\ 10^7$	$k_{act}=7.323\ 10^7$
Self-aligning ball bearing stiffness (N/m)	$k_{ceramicaxial}=4.391\ 10^6$ $k_{ceramicradial}=1.273\ 10^8$ $k_{steelaxial}=8.428\ 10^6$ $k_{steelradial}=1.134\ 10^8$	$k_{ceramicaxial}=4.391\ 10^6$ $k_{ceramicradial}=1.273\ 10^8$ $k_{steelaxial}=8.428\ 10^6$ $k_{steelradial}=1.134\ 10^8$	$k_{ceramicaxial}=4.391\ 10^6$ $k_{ceramicradial}=1.273\ 10^8$ $k_{steelaxial}=8.428\ 10^6$ $k_{steelradial}=1.134\ 10^8$
Linear rolling bearing stiffness (N/m) *Along x axis* *Along y axis*	$k_{x1}=1.246\ 10^{10}$ $k_{x2}=2.458\ 10^{10}$ $k_{y1}=6.571\ 10^9$ $k_{y2}=6.571\ 10^9$	$k_{x1}=1.246\ 10^{10}$ $k_{x2}=2.458\ 10^{10}$ $k_{y1}=6.571\ 10^9$ $k_{y2}=6.571\ 10^9$	$k_{x1}=1.246\ 10^{10}$ $k_{x2}=2.458\ 10^{10}$ $k_{y1}=6.571\ 10^9$ $k_{y2}=6.571\ 10^9$

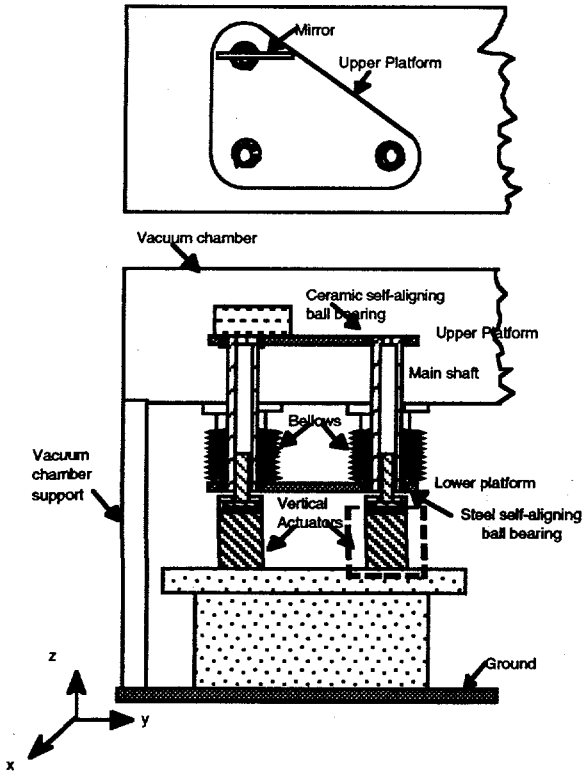

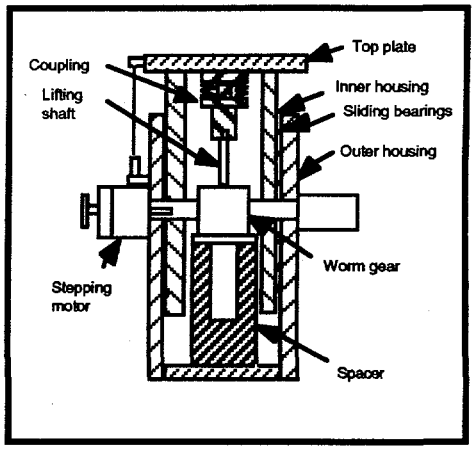

Figure 1 Schematic of the mirror support system. (Detailed drawing of the vertical actuator is shown on the right)

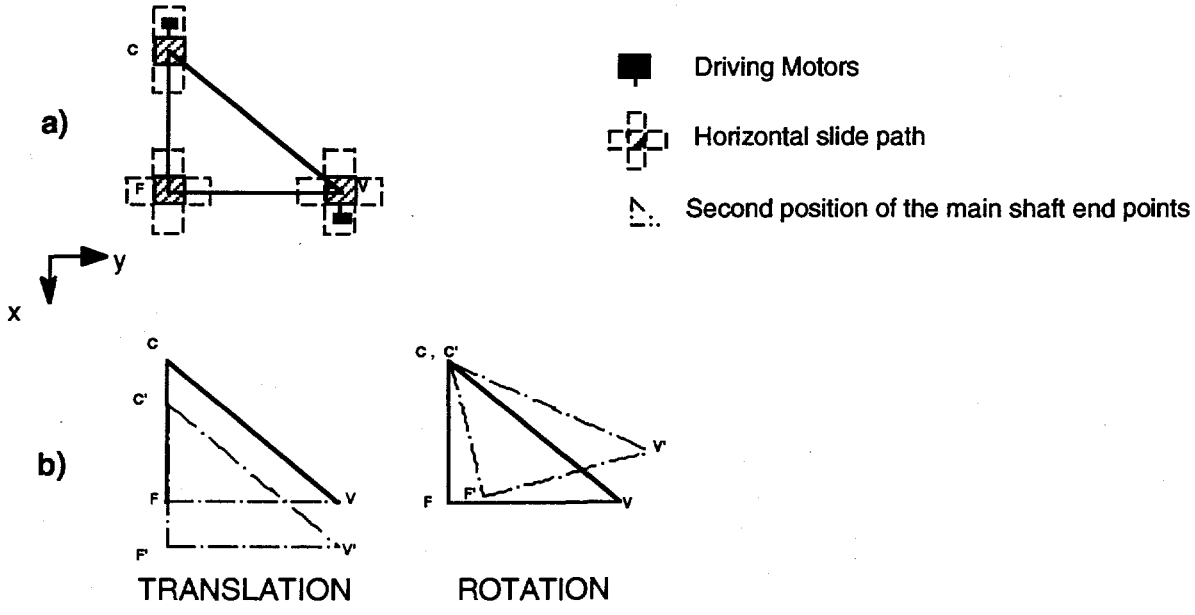

Figure 2 Top view of the horizontal slides demonstrating translational and rotational motion when the motors are driven.

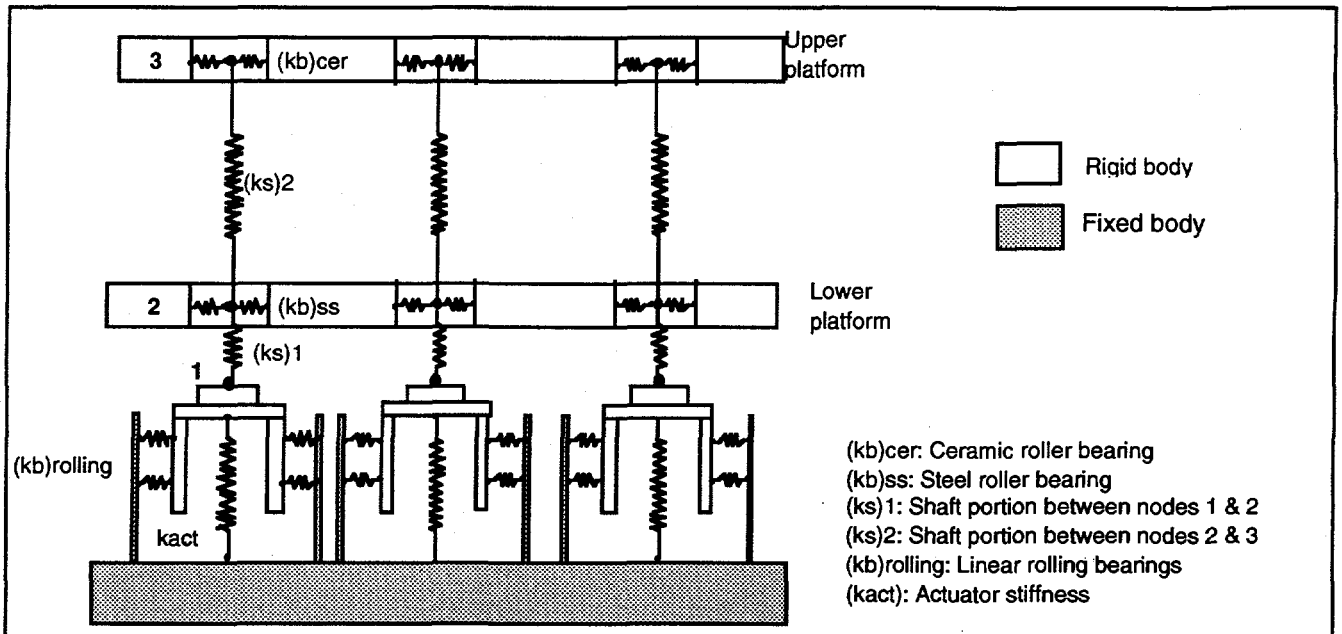

Figure 3 Schematic of the proposed model.

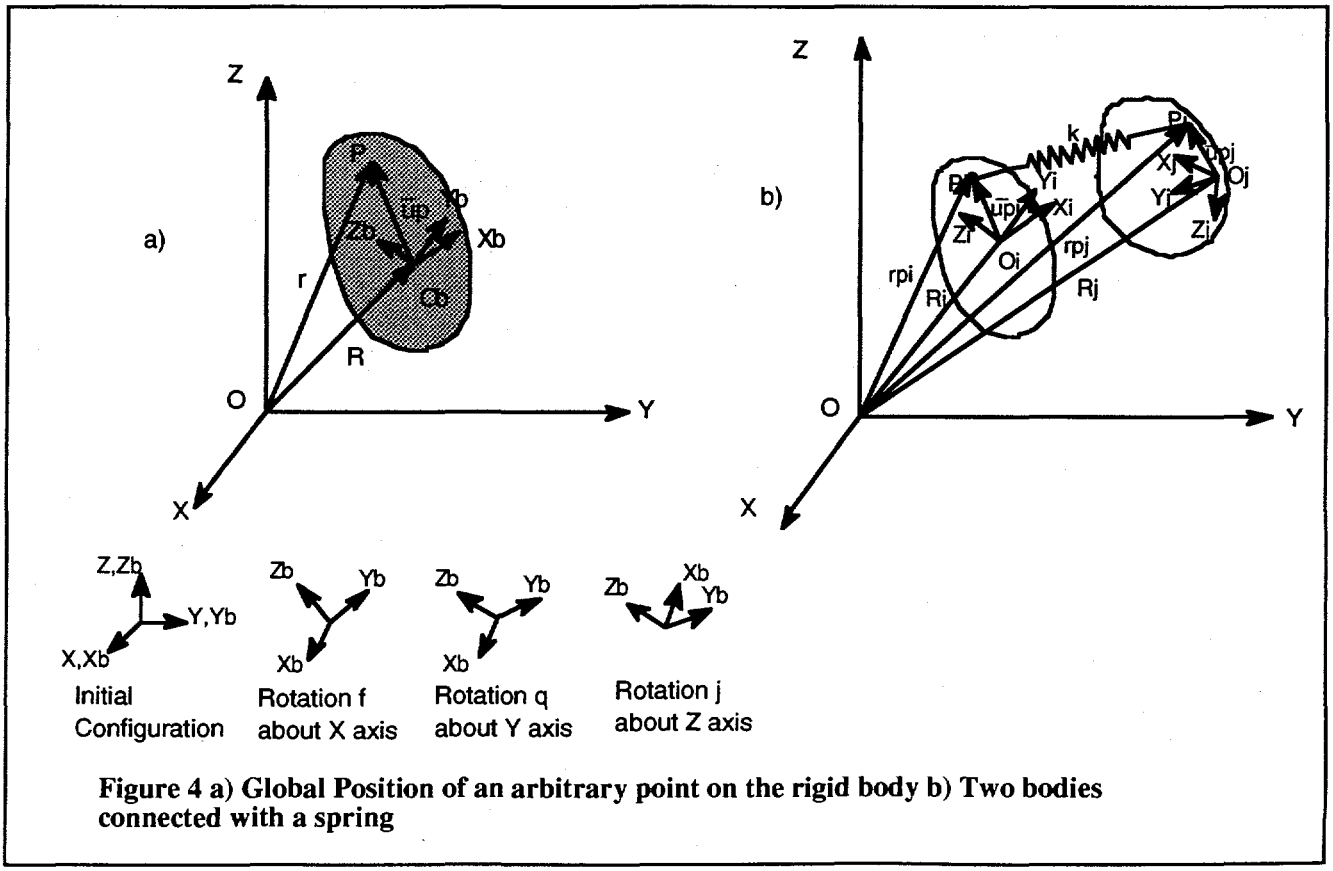

Figure 4 a) Global Position of an arbitrary point on the rigid body b) Two bodies connected with a spring

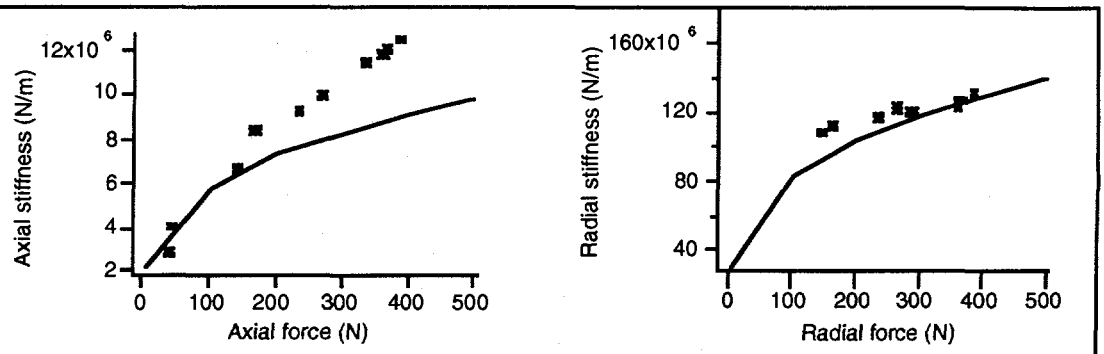

Figure 5 Comparison of experimental and theoretical results. (Markers show experimental results while continuous lines are used for theoretical results.)

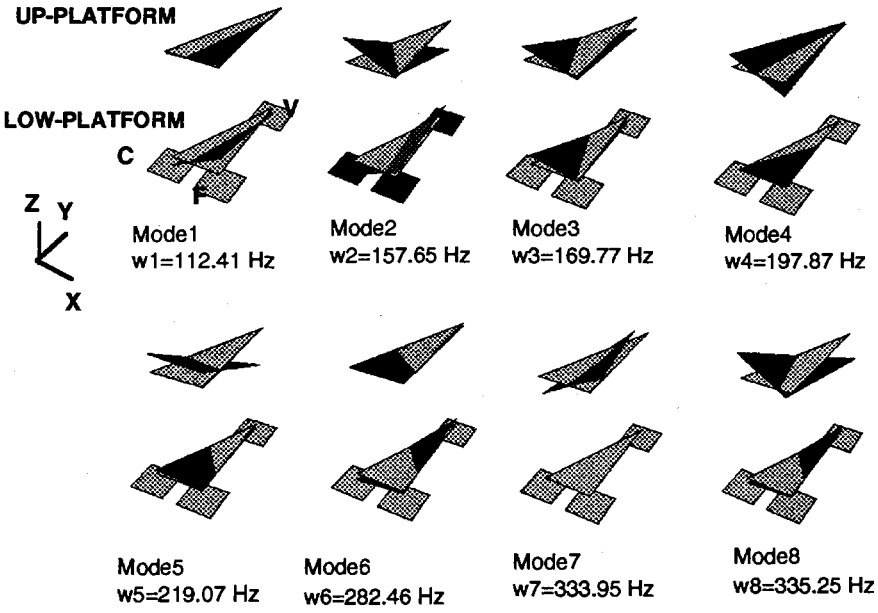

Figure 6 Mode shapes for the first 8 natural frequencies (grey and black denote undeformed and deformed, respectively).

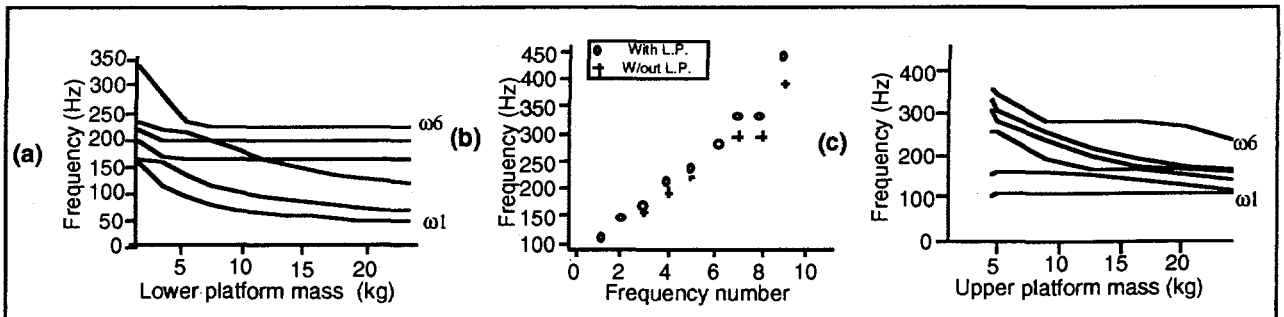

Figure 7 a) Change of resonance frequencies as a function of lower platform mass. b) Effect of removing lower platform. c) Change of frequencies as a function of upper platform mass.